

PAPER • OPEN ACCESS

An Improved Strategy for Modular Multilevel Converter at Low Speed Operation

To cite this article: Qifan Zeng *et al* 2018 *IOP Conf. Ser.: Mater. Sci. Eng.* **394** 042085

View the [article online](#) for updates and enhancements.

You may also like

- [Comparative Analysis of 5 level, 7 level and 9 level Half-Bridge Modular Multilevel Converter](#)
Jatin, Anshul Agarwal and Vinay Kumar Jadoun
- [Effect of Loss Distributions on the Balance of Capacitor Voltages in MMC Using Full Bridge Sub-Modules](#)
Chujiao Wang, Qin Wang, Chuyang Wang et al.
- [A Novel Capacitor Voltage Balancing Method for MMCs with Less Computation and Lower Switching Frequency](#)
Xin Gou, Jiping Lu and Wenling Deng



ECS
The
Electrochemical
Society
Advancing solid state &
electrochemical science & technology

DISCOVER
how sustainability
intersects with
electrochemistry & solid
state science research

An Improved Strategy for Modular Multilevel Converter at Low Speed Operation

Qifan Zeng*, Fei Xiao, Sheng Ai and Qiang Ren

National Key Laboratory of Science and Technology on Vessel Integrated Power System, Naval University of Engineering, Wuhan, China

*Corresponding author e-mail: shovenveryk@126.com

Abstract. One of the main problems of the Modular Multilevel Converter (MMC) for ship electric propulsion applications is the significant magnitude of capacitor voltage ripple at low speed operation. The commonly used solution is harmonic injection. In this paper, the injection rules are explored through the dynamic relationship of MMC in a comprehensive way, and the harmonic characteristics of injection current are derived. Furthermore, the circulating current controller is modified according to the harmonics of injected current with changing frequency, which reduces the ripple of capacitor voltage effectively in a wide speed range. Simulation results are shown to demonstrate the effectiveness of the proposed method.

1. Introduction

The Modular Multilevel Converter (MMC) has been widely used in the field of high voltage direct current (HVDC) transmission [1, 2], and has attracted increasing attention for the application of medium-voltage adjustable-speed motor drive [3, 4, 5]. The great potential of MMC for ship electric propulsion has been mentioned in [6]. The main challenge of the application of MMC-based drive system is the suppression of capacitor voltage ripple at low speed operation.

In order to suppress the voltage ripples of submodule (SM) capacitor which increase significantly as the output frequency decreases, several schemes have been adopted. Harmonic injection is the most mature method at present. The values of injected components are usually derived from MMC's arm energy relations. Several components are neglected in the derivation process which make the derivation result lack of comprehensiveness.

The injected circulating current is regulated by the circulating current controller which also controls the even harmonics caused by MMC's mechanism. The performance of the circulating current controller is related to the control accuracy of the injected current. Many control strategies have been used in the design of current controller, such as repetitive control [7], model predictive control [8], and multiple quasi-resonant control [9], but they are only designed to regulate the even harmonics at the rated frequency. Meanwhile some other literatures like [10], [11] put emphasis on the control of the injected current but neglect the even harmonics which needs to be regulated at the same time. In [12], the current controller contains six resonant controllers to regulate the second harmonic and injected harmonics at low speed operation, but it is not suitable with the changing frequency.

In this paper, the injection rules are explored through the relations of mathematical model, and the proposed formula of harmonic injection is derived from the rules. The circulating current controller is



modified according to the changing frequency of injected reference current, which improves tracking accuracy. Finally, the novel method shows the superior performance with respect to the reduced magnitude of capacitor voltage ripple in a wide speed range. Simulation results verified the validity and effectiveness of the method.

2. The operating principles of MMC

The circuit configuration of a three-phase MMC based on half-bridge submodule (HB-SM) for motor drive is shown in Fig.1. Each phase consists of the upper arm and the lower arm, and each arm has a buffer inductor L and N identical SMs connected in series. The half-bridge SM contains one capacitor C and two power devices, S_1 and S_2 . Each SM can be bypassed or inserted by controlling the switch states of S_1 and S_2 .

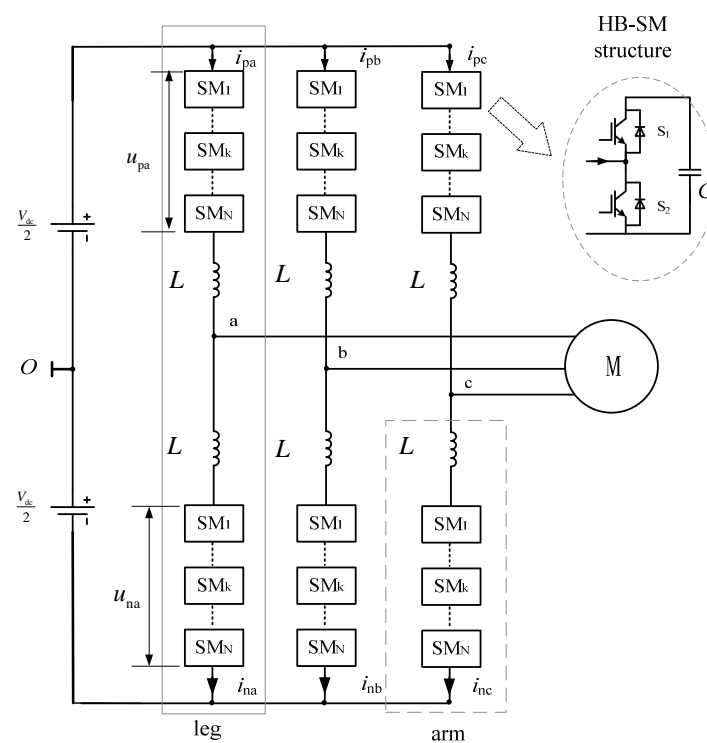


Figure 1. HB-SM based MMC feeding a three-phase motor

As depicted in Fig.1, assume that MMC is three-phase symmetry and the voltage relations along x-phase loop can be expressed as (1), where 'x' represents a-, b- or c-phase:

$$\begin{cases} u_{px} = U_{dc} / 2 - u_x - L \frac{di_{px}}{dt} \\ u_{nx} = U_{dc} / 2 + u_x - L \frac{di_{nx}}{dt} \end{cases} \quad (1)$$

Here, U_{dc} is the DC source voltage, u_x is output voltage of x-phase, u_{px} , u_{nx} are the upper and lower arm voltages, respectively. i_{px} , i_{nx} are arm currents.

The PWM reference waveforms of the upper and lower arms are given by

$$\begin{cases} n_{px} = u_{px}^* / U_{dc} = \frac{U_{dc} / 2 - u_x^* - u_{zx}^*}{U_{dc}} \\ n_{nx} = u_{nx}^* / U_{dc} = \frac{U_{dc} / 2 + u_x^* - u_{zx}^*}{U_{dc}} \end{cases} \quad (2)$$

Here, the harmonic component of the order of the switching frequency are assumed to be neglected. u_{pa}^* , u_{na}^* are the voltage reference of upper and lower arm. The output voltage reference u_x^* is obtained by the output current control. The offset voltage reference u_{zx}^* is obtained by the circulating current control to drive the circulating current i_{zx} .

Assume that all SM capacitor voltages within each arm are equal during operating, all SMs within each arm can be considered as a multi-level controlled voltage source. The relationship between arm voltages and the PWM reference waveforms is presented as (3):

$$\begin{cases} u_{px} = n_{px} u_{px}^\Sigma \\ u_{nx} = n_{nx} u_{nx}^\Sigma \end{cases} \quad (3)$$

In (3), u_{px}^Σ , u_{nx}^Σ is respectively the sum of all SMs' capacitor voltages in the upper arm and the lower arm. The dynamics of u_{px}^Σ and u_{nx}^Σ are obtained:

$$\begin{cases} C \frac{du_{px}^\Sigma}{dt} = N n_{px} i_{px} \\ C \frac{du_{nx}^\Sigma}{dt} = N n_{nx} i_{nx} \end{cases} \quad (4)$$

The dynamic of circulating current is obtained:

$$L \frac{di_{zx}}{dt} = \frac{U_{dc}}{2} - \frac{u_{px} + u_{nx}}{2} \quad (5)$$

3. The dynamic analysis of MMC with harmonic injection

Since the ripple magnitude of the SM capacitor voltages is inversely proportional to AC output frequency of MMC, some methods are needed to suppress voltage ripple of the SM capacitor under low speed operation. The common solution of state of art is the harmonic injection, which nullifies the low-frequency components of the capacitor voltage ripple by injecting high-frequency (relative to AC output frequency) common-mode voltages and circulating currents with the same frequency. Among the previous method, the shape of injected components derived from MMC's arm energy relations, this paper will explore the injection rules through the relations of mathematical model.

The injected circulating current is denoted as i_{z-h} , and injected common-mode voltage is denoted as u_{cm}^* . Assuming the second harmonic of circulating current is suppressed to a negligible level, then the arm currents can be expressed by

$$\begin{cases} i_{px} = I_{dx} + i_{z-h} + \frac{1}{2}i_x \\ i_{nx} = I_{dx} + i_{z-h} - \frac{1}{2}i_x \end{cases}, \quad (6)$$

Where I_{dx} is the DC component of circulating current in x-phase and i_x is the AC-side current.
 $i_x = I_s \sin(\omega t - \varphi)$.

Assuming $u_x^* = \frac{mU_{dc}}{2} \sin(\omega t)$, the PWM reference waveforms can be rewritten as:

$$\begin{cases} n_{px} = \frac{U_{dc}/2 - u_x^* - u_{cm}^* - u_{zx}^*}{U_{dc}} = \frac{U_{dc}/2 - mU_{dc}/2 \cdot \sin(\omega t) - u_{cm}^* - u_{zx}^*}{U_{dc}} \\ n_{nx} = \frac{U_{dc}/2 + u_x^* + u_{cm}^* - u_{zx}^*}{U_{dc}} = \frac{U_{dc}/2 + mU_{dc}/2 \cdot \sin(\omega t) + u_{cm}^* - u_{zx}^*}{U_{dc}} \end{cases}. \quad (7)$$

The relation of the SM capacitor current of x-phase can be expressed by

$$C \frac{du_{px}^\Sigma}{dt} = \frac{N}{2} [I_{dx} + \frac{1}{2}I_s \sin(\omega t - \varphi) + i_{z-h}] [1 - m \sin(\omega t) - \frac{2u_{cm}^*}{U_{dc}} - \frac{2u_{zx}^*}{U_{dc}}], \quad (8)$$

$$C \frac{du_{nx}^\Sigma}{dt} = \frac{N}{2} [I_{dx} - \frac{1}{2}I_s \sin(\omega t - \varphi) + i_{z-h}] [1 + m \sin(\omega t) + \frac{2u_{cm}^*}{U_{dc}} - \frac{2u_{zx}^*}{U_{dc}}]. \quad (9)$$

Hence, u_{px}^Σ and u_{nx}^Σ can be derived from (8) and (9):

$$\begin{aligned} u_{px}^\Sigma = & u_{p0}^\Sigma + \frac{N}{2C} \int I_{dx} - \frac{1}{4}mI_s \cos \varphi dt + \frac{NmI_{dx} \cos \omega t}{2\omega C} \\ & - \frac{NI_s \cos(\omega t - \varphi)}{4\omega C} + \frac{mNI_s \sin(2\omega t - \varphi)}{16\omega C} \\ & + \frac{N}{2C} \int \left\{ \begin{aligned} & i_{z-h} \left(1 - \frac{2u_{cm}^*}{U_{dc}} - \frac{2u_{zx}^*}{U_{dc}} \right) - i_{z-h} m \sin(\omega t) \\ & - \left[I_{dx} + \frac{1}{2}I_s \sin(\omega t - \varphi) \right] \left(\frac{2u_{cm}^*}{U_{dc}} + \frac{2u_{zx}^*}{U_{dc}} \right) \end{aligned} \right\} dt, \quad (10) \end{aligned}$$

$$\begin{aligned}
u_{nx}^{\Sigma} = & u_{n0}^{\Sigma} + \frac{N}{2C} \int I_{dx} - \frac{1}{4} m I_s \cos \varphi dt - \frac{N m I_{dx} \cos \omega t}{2\omega C} \\
& + \frac{N I_s \cos(\omega t - \varphi)}{4\omega C} + \frac{m N I_s \sin(2\omega t - \varphi)}{16\omega C} \\
& + \frac{N}{2C} \int \left\{ \begin{aligned} & i_{z-h} \left(1 + \frac{2u_{cm}^*}{U_{dc}} - \frac{2u_{zx}^*}{U_{dc}} \right) + i_{z-h} m \sin(\omega t) \\ & + \left[I_{dx} - \frac{1}{2} I_s \sin(\omega t - \varphi) \right] \left(\frac{2u_{cm}^*}{U_{dc}} - \frac{2u_{zx}^*}{U_{dc}} \right) \end{aligned} \right\} dt. \quad (11)
\end{aligned}$$

Here, u_{p0}^{Σ} and u_{n0}^{Σ} are the initial values of u_{px}^{Σ} and u_{nx}^{Σ} , whose values are both U_{dc} . The second terms of right-hand side in (10) and (11) have to be zero in order to maintain the mean value of each SM capacitor voltage as a constant.

The low-frequency component of u_{px}^{Σ} and u_{nx}^{Σ} which should be nullified are divided into two parts: the fundamental component with the same magnitude and opposite phase between the upper and lower arms and the second harmonic component with the same value between the upper and lower arms.

The only way to nullify the second harmonic component is to generate a second harmonic circulating current i_{z-2} by controlling u_{zx}^* , and its value is expressed as

$$i_{z-2} = -\frac{m I_s \cos(2\omega t - \varphi)}{4}. \quad (12)$$

Thus, (8) and (9) are rewritten as

$$\begin{aligned}
C \frac{du_{px}^{\Sigma}}{dt} = & \frac{N}{2} I_{dx} - \frac{N}{8} m I_s \cos \varphi - \frac{N}{2} m I_{dx} \sin \omega t + \frac{N}{4} I_s \sin(\omega t - \varphi) \\
& + \frac{N}{2} i_{z-2} \left[-m \sin(\omega t) - \frac{2u_{cm}^*}{U_{dc}} - \frac{2u_{zx}^*}{U_{dc}} \right] \\
& + \frac{N}{2} i_{z-h} \left(1 - \frac{2u_{cm}^*}{U_{dc}} - \frac{2u_{zx}^*}{U_{dc}} \right) - \frac{N}{2} i_{z-h} m \sin(\omega t) \\
& - \frac{N}{2} \left[I_{dx} + \frac{1}{2} I_s \sin(\omega t - \varphi) \right] \left(\frac{2u_{cm}^*}{U_{dc}} + \frac{2u_{zx}^*}{U_{dc}} \right), \quad (13)
\end{aligned}$$

$$\begin{aligned}
C \frac{du_{nx}^{\Sigma}}{dt} &= \frac{N}{2} I_{dx} - \frac{N}{8} m I_s \cos \varphi + \frac{N}{2} m I_{dx} \sin \omega t - \frac{N}{4} I_s \sin(\omega t - \varphi) \\
&+ \frac{N}{2} i_{z_{-2}} \left[m \sin(\omega t) + \frac{2u_{cm}^*}{U_{dc}} - \frac{2u_{zx}^*}{U_{dc}} \right] \\
&+ \frac{N}{2} i_{z_{-h}} \left(1 + \frac{2u_{cm}^*}{U_{dc}} - \frac{2u_{zx}^*}{U_{dc}} \right) + \frac{N}{2} i_{z_{-h}} m \sin(\omega t) \\
&+ \frac{N}{2} \left[I_{dx} - \frac{1}{2} I_s \sin(\omega t - \varphi) \right] \left(\frac{2u_{cm}^*}{U_{dc}} - \frac{2u_{zx}^*}{U_{dc}} \right)
\end{aligned} \tag{14}$$

Therefore, the low-frequency component in (13) and (14) can be nullified by the low frequency component of $i_{z_{-h}} u_{cm}^*$. The relation can be derived as (15).

$$i_{z_{-h}} u_{cm}^* \Big|_{low\ freq.} = -\frac{1}{2} m (I_{dx} + i_{z_{-2}}) U_{dc} \sin \omega t + \frac{1}{4} I_s U_{dc} \sin(\omega t - \varphi) \tag{15}$$

In order to satisfy the relationship of (15), $i_{z_{-h}}$ can be defined by (16) and ω_h represents the angular frequency of injected high-frequency components.

$$i_{z_{-h}} = \left[-\frac{1}{2} m (I_{dx} + i_{z_{-2}}) U_{dc} \sin \omega t + \frac{1}{4} I_s U_{dc} \sin(\omega t - \varphi) \right] \frac{\sin(\omega_h t)}{U_{cm}} \tag{16}$$

Under the consideration of (16) and (12), the current $i_{z_{-h}}$ has 4 kinds of frequency component which are $\omega_h - \omega$, $\omega_h + \omega$, $\omega_h + 3\omega$ and $\omega_h - 3\omega$, the current $i_{z_{-2}}$ has DC component and second harmonic component (2ω).

4. The proposed circulating current controller

For the harmonic injection method, the injected common-mode voltage can be realized directly by changing the reference modulation wave, but the accurate injection of circulating current has to be guaranteed by the high-performance current controller. Therefore, the following emphasis is placed on the design of the circulating current controller.

4.1. The quasi-resonant controller

As mentioned above, the circulating current controller need to control DC component and multiple harmonic components. Although ω_h is fixed, the output frequency is ranged from 0 to the rated frequency in the MMC drive system, the angular frequency, i.e., 2ω , $\omega_h - \omega$, $\omega_h + \omega$, $\omega_h + 3\omega$ and $\omega_h - 3\omega$ are not constants. Considering the narrow bandwidth of the resonant controller and non-ideal factors such as quantization error, the resonant controller may lose its potency. According to this case, this paper uses the quasi-resonant controller with wider band instead.

4.2. Simplification of the controller

For making the circulating current controller more practical, the current controller should be simplified. It is known obviously from (16) that the magnitudes of $\omega_h + 3\omega$ and $\omega_h - 3\omega$ are much less than the

other components and can be neglected. So only three resonant controllers for 2ω , $\omega_h - \omega$ and $\omega_h + \omega$ are needed to regulate circulating current.

The transfer function from u_z to i_z can be expressed as

$$G_z(s) = \frac{i_z(s)}{u_z(s)} = \frac{1}{R + sL}. \quad (17)$$

Here, R is the line impedance of the arm.

The transfer function of circulating current controller at low-speed operation is expressed as (18).

$$G_{\text{PIRC}}(s) = K_p + K_i / s + \frac{K_R s}{s^2 + 2\omega_c s + \omega^2} + \frac{K_R s}{s^2 + 2\omega_c s + (\omega_{c_h1})^2} + \frac{K_R s}{s^2 + 2\omega_c s + (\omega_{c_h2})^2}. \quad (18)$$

Here, $\omega_{c_h1} = \omega_h - \omega$, $\omega_{c_h2} = \omega_h + \omega$, ω_c is the cutoff frequency, K_p , K_i and K_R are the gain parameter of the controller.

The output frequency is nearly zero at startup operation. Under this circumstance, the bandwidths of the two resonant controllers for $\omega_h - \omega$ and $\omega_h + \omega$ will be overlapped, the second harmonic and DC component can be controlled together by the proportional-integral (PI) controller.

In order to analyze the overlap degree of the bands of controllers at different operation, the spectrum characteristics of $G_{\text{PIRC}}(s)G_z(s)$ when $\omega_h = 100 \cdot 2\pi$ and ω differs from 2π to 20π are shown in Fig.2.

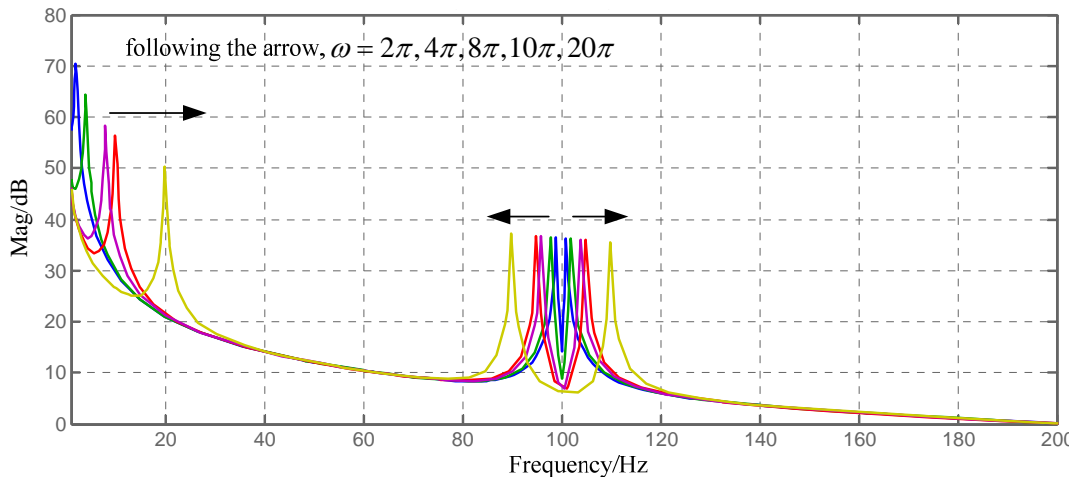


Figure 2. The spectrum characteristics of $G_{\text{PIRC}}(s)G_z(s)$

As shown in Fig.2, when $\omega < 8\pi$, the overlap phenomenon is serious, in this case, the resonant controller for 2ω can be removed and the resonant controllers for $\omega_h - \omega$ and $\omega_h + \omega$ can be merged into one. When $\omega \geq 8\pi$, the controller can be designed as (18).

5. Simulation results

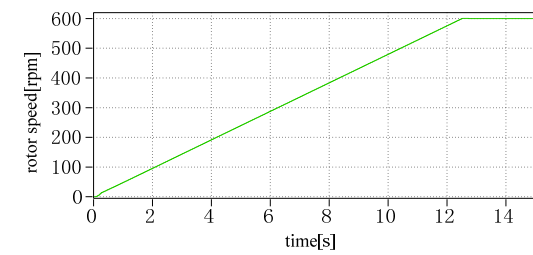
To verify the validity of the proposed control strategy, a three-phase MMC based induction motor (IM) drive system has been implemented as shown in Fig.1. The carrier phase shift modulation with sorting method in [13] is applied in this system. The parameters are listed in Table 1. This system is simulated in PLECS environment.

Table 1. System Parameters

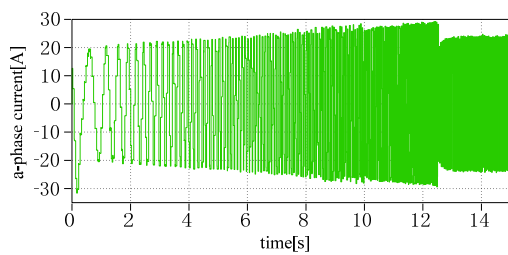
MMC parameters	
SM capacitance C	6.3 mF
Arm inductance L	2.5 mH
DC-source voltage U_{dc}	400 V
Number of SMs per arm N	4
Carrier frequency	500 Hz
Rated output frequency	20 Hz
Rated voltage of SM capacitor u_c	100 V
IM parameters	
Rated RMS line current I_{rated}	25 A
Rated RMS voltage (line-to-line) U_{rated}	250 V
Rated rotational speed ω_{rated}	600 rpm
Pole pair number pp	2

The operation from standstill to rated speed with the proposed method is shown in Fig.3 while the operation with traditional method [12] is shown in Fig.4. In order to be close to the practical application of ship propulsion, the load torque is set in proportional to the square of the speed. After $t = 10$ s, the injection method is removed and the operating mode changes to the normal operation mode.

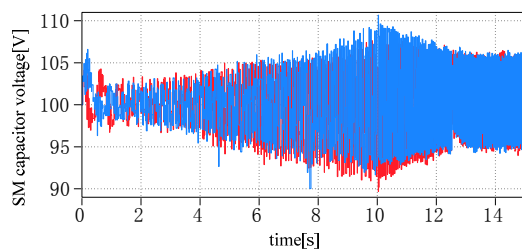
As shown in Figs. 3-4, the two methods show similar performance in general. However, the ripple magnitude in Fig.4 is larger when the motor has just started. The reason is depicted in Section 4.2, the frequency of second harmonic is too low at the beginning, which causes the band overlap of PI controller and resonant controller, finally results in great control gain of circulating current at low frequencies. Therefore, the simulation result shows that the proposed method performs much steady on voltage ripple reduction in a wide speed range compared with the traditional method.



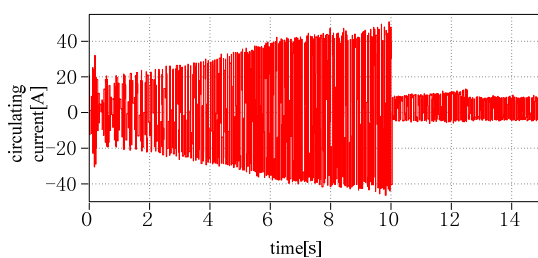
(a)



(b)

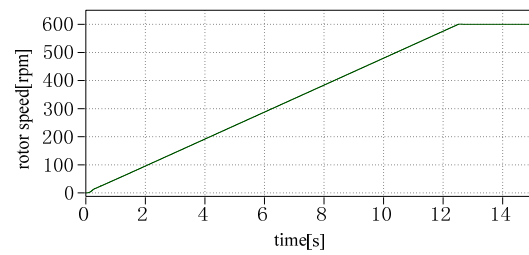


(c)

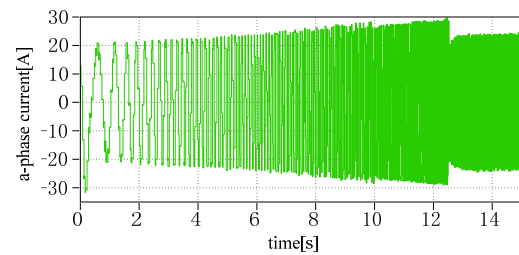


(d)

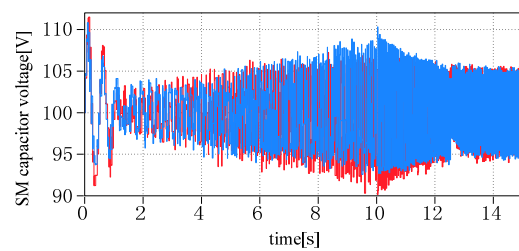
Figure 3. MMC waveforms for the proposed method: (a) rotor speed, (b) a-phase current, (c) two SM capacitor voltages in a-phase, (d) circulating current of a-phase



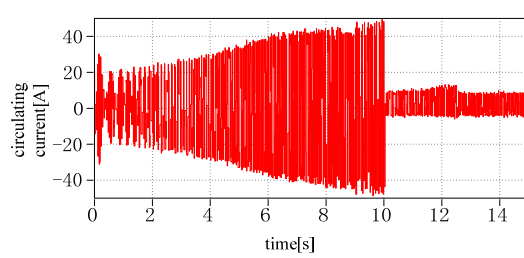
(a)



(b)



(c)



(d)

Figure 4. MMC waveforms for the traditional method: (a) rotor speed, (b) a-phase current, (c) two SM capacitor voltages in a-phase, (d) circulating current of a-phase

6. Conclusion

In the paper, an improved harmonic injection method for reduction of MMC capacitor voltage ripples under low speed operation is presented. The dynamic relationship of MMC is analyzed in a comprehensive way and the harmonic characteristics of injection current are derived. Furthermore, the circulating current controller is modified according to the harmonics of injected current with changing frequency. Using the proposed method, the ripple of each SM capacitor voltage can be maintained within an allowable range. Furthermore, the proposed method shows lower ripple magnitudes at nearly

zero speed than traditional method. The effectiveness and validity have been verified by Simulation results.

Acknowledgments

This work was financially supported by National Natural Science Foundation of China (51407189), National Basic Research Program of China (973 Program, 2015CB251004).

References

- [1] Davies M., et al. "HVDC plus—Basics and Principle of Operation." Special Edition for Cigré Exposition. 2008.
- [2] W Tingfang, W Zhinong, S Guoqiang, et al. "New prospects of modular multilevel converter applied to voltage source converter high voltage direct current transmission." *High Voltage Engineering* 38.5 (2012): 1243-1252.
- [3] A. Antonopoulos, L. Angquist, S. Norrga, K. Ilves, L. Harnfors, H.-P. Nee, "Modular multilevel converter ac motor drives with constant torque from zero to nominal speed." *IEEE Transactions on Industry Applications* 50.3 (2014): 1982-1993.
- [4] Jung Jae-Jung, Hak-Jun Lee, and Seung-Ki Sul. "Control strategy for improved dynamic performance of variable-speed drives with modular multilevel converter." *IEEE Journal of Emerging and Selected Topics in Power Electronics* 3.2 (2015): 371-380.
- [5] A. Antonopoulos, L. Angquist, L. Harnfors, H. Nee, "Optimal selection of the average capacitor voltage for variable-speed drives with modular multilevel converters." *IEEE transactions on power electronics* 30.1 (2015): 227-234.
- [6] M. Spichartz, V. Staudt, A. Steimel, "Modular multilevel converter for propulsion system of electric ships," *Proc. IEEE Electr. Ship Technol. Symp.*, pp. 237-242, 2013.
- [7] L. He, K. Zhang, J. Xiong, S. Fan. "A repetitive control scheme for harmonic suppression of circulating current in modular multilevel converters," *IEEE transactions on power electronics* 30.1 (2015): 471-481.
- [8] Huancheng Lin, Zhixin Wang, Li Shi, Binfeng Lu. "Model predictive control method of modular multilevel converter based on hierarchical control." *High Voltage Engineering* 42.1 (2016): 143-152.
- [9] Xiaojie Wu, Yang Chao, and Gong Zheng, et al. "Simplified circulating current suppressing strategy for MMC based on multi-resonant controller." *Transactions of China Electrotechnical Society* 31.13 (2016): 74-81.
- [10] Shengfang Fan. "Research on key technologies for modular multilevel converters". PhD diss., Huazhong University of Science & Technology (2014).
- [11] Qianming Xu, An Luo, Fujun Ma, et al. "The control scheme of modular multilevel converter with tuned filter operating at low frequency." *Proceeding of the CSEE*, 2016, 36 (2): 489-498.
- [12] Jung, Jae-Jung, Hak-Jun Lee, and Seung-Ki Sul. "Control of the modular multilevel converter for variable-speed drives." *Power Electronics, Drives and Energy Systems (PEDES), 2012 IEEE International Conference on.* IEEE, 2012.
- [13] L. Zixin, W. Ping, Z. Haibin, C. Zunfang, and L. Yaohua, "An Improved Pulse Width Modulation Method for Chopper-Cell-Based Modular Multilevel Converters," *Power Electronics, IEEE Transactions on*, vol. 27, pp. 3472-3481, 2012.